

# Quantum bath augmented stochastic nonequilibrium atomistic simulations for molecular heat conduction

Renai Chen,<sup>1,2, a)</sup> Mohammadhasan Dinpajoo,<sup>3</sup> and Abraham Nitzan<sup>1,4</sup>

<sup>1)</sup>*Department of Chemistry, University of Pennsylvania, Philadelphia, PA 19104,  
USA*

<sup>2)</sup>*Theoretical Division and Center for Nonlinear Studies,  
Los Alamos National Laboratory, Los Alamos, NM, 87544,  
USA*

<sup>3)</sup>*Physical and Computational Sciences Directorate, Pacific Northwest National  
Laboratory, WA 99352 USA*

<sup>4)</sup>*School of Chemistry, Tel Aviv University, Tel Aviv 69978,  
Israel*

Classical molecular dynamics (MD) has been shown to be effective in simulating heat conduction in certain molecular junctions since it inherently takes into account some essential methodological components which are lacking with quantum Landauer-type transport model, such as many-body full force-field interactions, anharmonicity effects and nonlinear responses for large temperature biases. However, the classical mechanics reaches its limit in the environments where the quantum effects are significant (e.g. with low-temperatures substrates, presence of extremely high frequency molecular modes). Here, we present an atomistic simulation methodology for molecular heat conduction that incorporates the quantum Bose-Einstein statistics into an “effective temperature” in the form of modified Langevin equation. We show that the results from such a quasi-classical effective temperature (QCET) MD method deviates drastically when the baths temperature approaches zero from classical MD simulations and the results converge to the classical ones when the bath approaches the high-temperature limit, which makes the method suitable for full temperature range. In addition, we show that our quasi-classical thermal transport method can be used to model the conducting substrate layout and molecular composition (e.g. anharmonicities, high-frequency modes). Anharmonic models are explicitly simulated via the Morse potential and compared to pure harmonic interactions, to show the effects of anharmonicities under quantum colored bath setups. Finally, the chain length dependence of heat conduction is examined for one-dimensional polymer chains placed in between quantum augmented baths.

---

<sup>a)</sup>Electronic mail: renaic@sas.upenn.edu

## I. INTRODUCTION

Heat transport in molecular systems is of great importance not only because it is an important subfield of nanoscale heat transfer<sup>1-3</sup> which promises optimized microscopic heat management, but also for its significant roles in molecular electronics, novel thermal-electric interactions and phononic computings.<sup>4-14</sup> Substrate-molecule-substrate type molecular junction (MJ) structures are the most prevalent testing grounds for both theoretical and experimental studies of molecular heat conduction.<sup>6,15-20</sup> Recent experimental advances on single-molecule junction (SMJ) high-precision heat conduction measurements,<sup>21,22</sup> has put an urgency of finding a comprehensive and reliable theoretical approach and numerical implementation, so that heat conductions in SMJ can be accurately and systematically investigated.

One of the dominant theoretical methodologies for thermal transport in MJs is the Nonequilibrium Green's Function (NEGF) method. In principle, such an approach can capture the full dynamics of the transport properties at steady-state. This approach is straightforward to implement in harmonic models. However, in practice, the harmonic approximation is often made to lower the computational costs and simplify the calculations.<sup>15,21,23-26</sup> Though such an approximation may still be reasonable for low temperature environments, its applicability in higher temperatures or systems with high anharmonicities could be problematic. On the other hand, the long-standing trajectory-based molecular dynamics (MD) has been used to simulate thermal conductivities of various nanoscale materials.<sup>18,27-36</sup> Its rich pool of parameterized complex systems that include many-body interactions and comparatively low computational costs make it suitable for simulating realistic systems where anharmonic effects could be important.

Indeed, a GROMACS-based computational toolkit that utilizes stochastic baths and sub-

strate filterings has been recently developed to simulate heat conduction across molecular junctions of different topologies and has been shown to be accurate and reliable for room temperature settings.<sup>37</sup> Nonetheless, the classical MD-based method loses its predicting power when the temperatures of the leads are pushed to a much lower end (e.g. 25K at one side of the junction) and the conductance deviates greatly from the quantum calculations.<sup>16,37</sup> One of the main reasons for such inaccuracy is the inability of classical mechanics in capturing the dominant quantum effect at low temperatures which primarily arises from quantum Bose-Einstein distribution.

Recently, there have been research efforts aimed to introduce quantum bath effects in non-equilibrium spin-boson (NESB) model for molecular heat transports,<sup>38</sup> in which significant differences are found between the samplings of classical and quantum baths. In addition, methodological development efforts have been put into blending quantum effects into classical MD using generalized Langevin equation<sup>39</sup> (GLE) and an attempt to implement such a method for the thermal transport processes in molecular junctions has been reported<sup>40</sup>. While such a quasi-classical approach seems to capture quantum effects of heat conduction for certain molecular junctions, the transformations between Fourier and time spaces of the noises could lead to heavy computational overheads. For large and realistic systems, further methodological developments are needed.

In this paper, circumventing painstaking assumptions and approximations of using GLE, we introduce a general mathematical framework that starts from Wiener-Khinchin-Einstein theorem to integrate quantum bath effects into MD simulations smoothly in the thermal transport simulations in the molecules, without sacrificing all the benefits inherited from classical simulations. The quantum fluctuation-dissipation relation appears to partly resemble GLE, but the clear pathway of implementing the stochastic force makes the method

conceptually and practically easy to be implemented. The implemented code contains the possibility to include colored noise. Such colored spectrum can be engineered based on the atomic parameters and coupling strengths depending on specific molecular systems under study. We will first elaborate on the detailed formalism of incorporating such effects through an effective temperature reconstruction to the Langevin dynamics. Then the method is demonstrated using toy models by looking into monatomic relaxation and diatomic heat conduction. In the meantime, a colored bath is simulated explicitly with tunable parameters of the bath internal degrees of freedom (e.g coupling constants). We finally test the quantum plus colored bath model on heat conduction with harmonic and anharmonic diatomic molecules and polymeric chain molecules, laying out foundations for the upcoming implementations of this general method into MD packages.

## II. METHODS AND FORMALISM

### A. Formalism for quasi-classical effective temperature molecular dynamics simulation

We start out with the Langevin's equation, for a single (bath) particle at position  $x$  (assuming one dimensional) under the potential  $V(x)$ .

$$m\ddot{x}(t) = -\frac{\partial V(x)}{\partial x} - m\gamma\dot{x} + R(t). \quad (1)$$

$\gamma$  is the friction term, and  $R(t)$  is the random fluctuation force acting on the particle. The friction  $\gamma$  and the random noise  $R$  are related by the fluctuation-dissipation theorem

$$\langle R(t)R(t') \rangle = 2m\gamma k_B \mathcal{T} \delta(t - t'), \quad (2)$$

where  $k_B$  is the Boltzmann constant and  $\mathcal{T}$  refers to the surrounding thermal environment or bath temperature.

Consider the random fluctuation term in more detail. Suppose we observe the system in time interval  $0 \leq t \leq T$  and expand  $R(t)$  in Fourier series.

$$R(t) = \sum_{n=-\infty}^{n=\infty} R_n e^{i\omega_n t} \quad (3)$$

$$\omega_n = \frac{2\pi n}{T}, \quad n = 0, \pm 1, \pm 2 \dots \quad (4)$$

$$R_n = \frac{1}{T} \int_0^T dt R(t) e^{-i\omega_n t} \quad (5)$$

The power spectrum can be written as<sup>41</sup>:

$$I_R(\omega) = \lim_{T \rightarrow \infty} \left( \frac{\sum_{n \in W_{\Delta\omega}} \langle |R_n|^2 \rangle}{\Delta\omega} \right); \quad (6)$$

where

$$W_{\Delta\omega} = \{n | \omega - \Delta\omega/2 \leq 2\pi n/T \leq \omega + \Delta\omega/2\}, \quad (7)$$

which can further change to

$$I_R(\omega) = \lim_{T \rightarrow \infty} \sum_{n \in W_{\Delta\omega}} \langle |R_n|^2 \rangle \delta(\omega - \omega_n); \quad \omega = \frac{2\pi n}{T}. \quad (8)$$

$I_R(\omega)\Delta\omega$  is the intensity of the random noise in the frequency range  $\omega \dots \omega + \Delta\omega$ , which is obtained by summing up the magnitudes of different components  $R_n^2$ .

The Wiener-Khintchine theorem states:

$$I_R(\omega) = \frac{1}{2\pi} \int_{-\infty}^{\infty} dt e^{-i\omega t} \langle R(t)R(0) \rangle. \quad (9)$$

Together with Eqn.(2), we get

$$I_R = \frac{m\gamma k_B \mathcal{T}}{\pi} \quad (10)$$

Here we want to find an approximate coarse-grained frequency resolution of the heat flux. To this end we divide the relevant frequency range  $\{0 \cdots \omega_{max}\}$  into  $N$  segments  $\Delta\omega = \omega_{max}/N$ .

For each such segment the random noise can be taken as,

$$\begin{aligned} R_n(t) &= \sqrt{\Delta\omega \frac{m\gamma k_B \mathcal{T}}{\pi}} \left( e^{i(\omega^{(n)}t + \phi_n)} + e^{-i(\omega^{(n)}t + \phi_n)} \right) \\ &= 2\sqrt{\Delta\omega \frac{m\gamma k_B \mathcal{T}}{\pi}} \cos(\omega^{(n)}t + \phi_n), \end{aligned} \quad (11)$$

where  $\omega^{(n)}$  is best chosen in the middle of the segment, that is  $\omega^{(n)} = (n - 1/2)\Delta\omega$  and  $\phi_n$  is the random phase, which will be averaged over multiple trajectories of different values.

Alternatively, each segment can be further divided into more than one frequency, say  $\{\omega_j^{(n)}\}, j = 1 \cdots M_n$  evenly distributed in the segments. In this case, the driving corresponding to the frequency segment  $n$  (between  $\omega_{n-1}$  and  $\omega_n$ ) is

$$R_n(t) = 2\sqrt{\frac{\Delta\omega}{M_n} \frac{m\gamma k_B \mathcal{T}}{\pi}} \sum_j \cos(\omega_j^{(n)}t + \phi_j). \quad (12)$$

The approximation lies in the assumption that the currents obtained from these drivings are additive, so that if we act together with two segments  $n$  and  $n+1$  the heat current will be the sum of the individual contributions. This is certainly so in harmonic systems but is only an approximation for anharmonic ones. The reason why the approximation might be feasible is that contributions from different segments will come with random phases so that mixed signal might average to zero when average over phases is done.

Qualitatively, one might conceptualize such an effective temperature represents frequency weighed thermal contribute from single bath mode versus uniform constant temperatures for classical MD (See Fig. 1 (a)). Together with the interplay between individual bath modes and molecular modes, the modified random force embodies the collective effect of all the vibrational modes within the thermal baths (like shown in Fig. 1 (b)) and its effect on the overall heat conduction, in a way analogous to Bose-Einstein population in

the Landauer's transport formalism.<sup>6</sup> Taking more frequencies is just like taking smaller segments. Therefore, the final expression for the random noise can be written as

$$R_n = 2\sqrt{\Delta\omega \frac{m\gamma k_B \mathcal{T}_{eff}(\omega^{(n)})}{\pi}} \cos(\omega^{(n)}t + \phi_n), \quad (13)$$

$$R(t) = \sum_n R_n(t),$$

where

$$\mathcal{T}_{eff}(\omega) = \frac{\hbar\omega/k_B}{e^{\hbar\omega/k_B\mathcal{T}} - 1}. \quad (14)$$

Different realizations of the random noise come from different choices of  $\phi_n$  for different choices of random noise. Note that now we have reformulated the random noise in our quasi-classical approach, we can do standard heat conduction without calculating frequency-resolved transmission coefficients, and the details about the heat current calculations (atomic local heat fluxes) can be found in a previous paper.<sup>37</sup> All that is required is to replace the random noise with a similar one but with a frequency-dependent effective temperature noting that the coupling of the system to the quantum bath involves explicitly the classical bath friction ( $\gamma$ ), the range of bath frequencies ( $\omega^{(n)}$ ), and Bose-Einstein distribution for the effective bath temperature ( $\mathcal{T}_{eff}$ ) all of which capture the bath quantum effects. In what follows, this method is called quasi-classical effective temperature (QCET) method. The QCET approach is shown to be accurate and computationally effective for simple models in molecular junctions and has been also demonstrated for one-dimensional polymeric systems.

## B. Atomistic design of colored bath

We will also consider heat transport between thermal baths characterized by the frequency dependence and cutoff given by the Debye model and their spectral properties. In such a



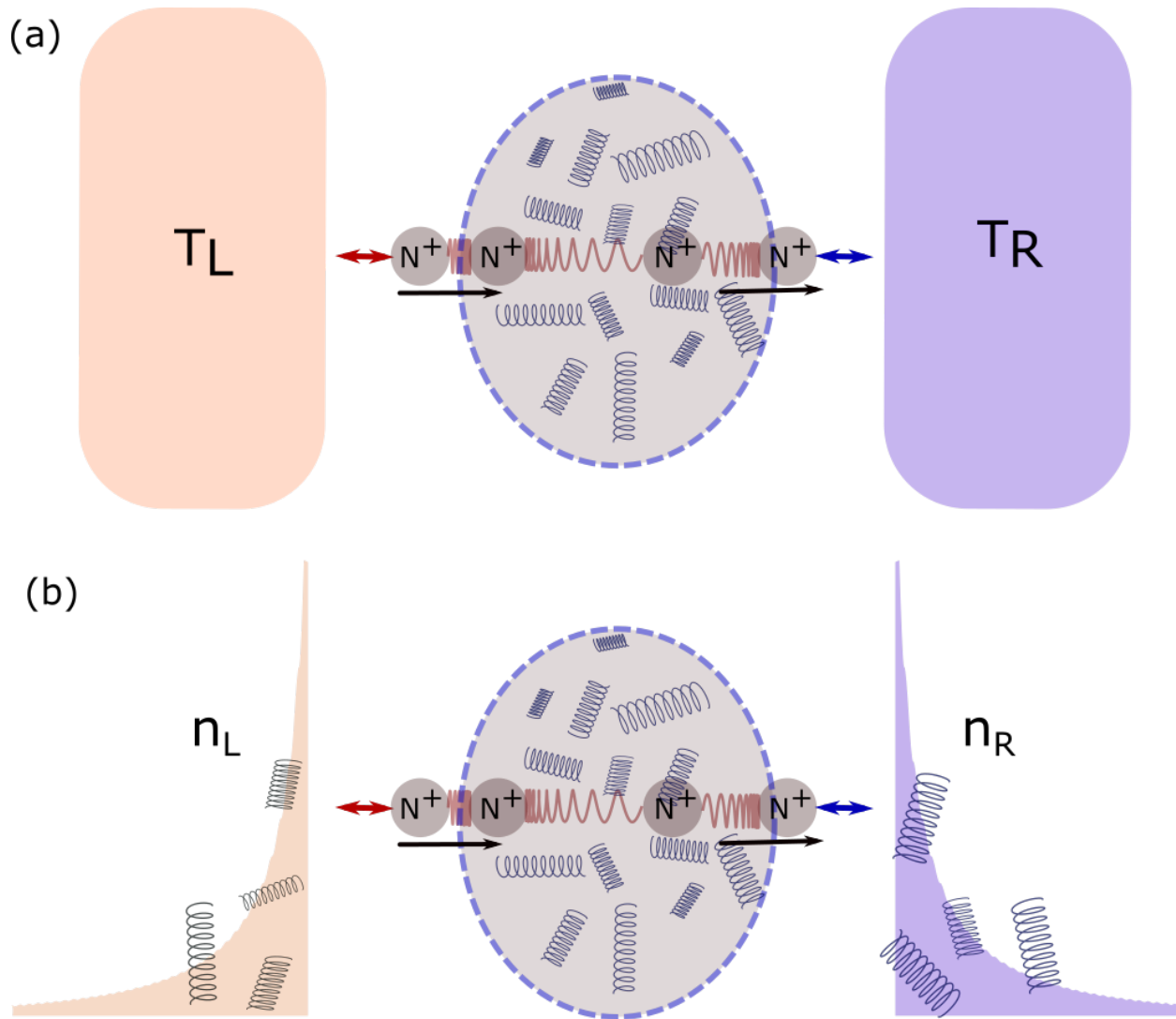


FIG. 1. Schematic diagrams of heat transport in molecular junctions across temperature biases.

(a) When the thermal baths are classical, meaning they do not differentiate different bath modes of different frequencies; (b) How the actual quantum baths look like: different bath modes weigh differently with respect to the corresponding temperatures, distributed according to Bose-Einstein phonon population distributions.

scenario, the quantum augmented bath model with modes of different frequencies contribute differently will provide more insights into the thermal transport dynamics than plain white-noise based classical MD approaches. Specifically, the spectrum behaves as  $\omega^2$  for small  $\omega$ 's,

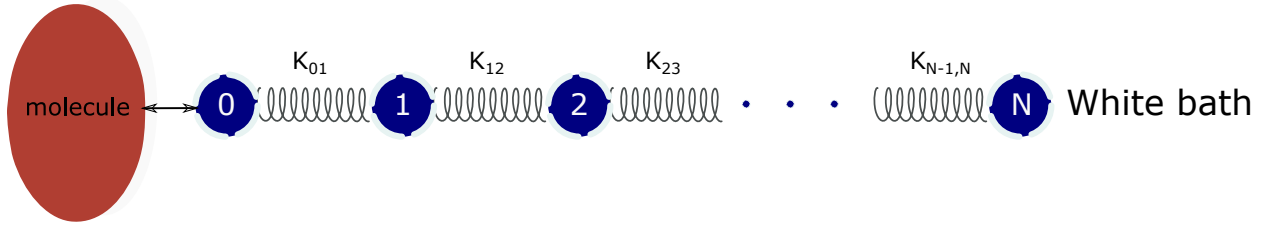


FIG. 2. Schematic drawing of the Debye bath composed of  $N$  atoms, attaching a bridge molecule on the left and white bath on the right.

and has a cutoff frequency ( $\omega_D$ ) when  $\omega \rightarrow \infty$ . One way to characterize such a colored bath spectrum is through mathematical filtering,<sup>42</sup> which implicitly incorporates the color of the bath into the Generalized Langevin equation. Another category of methods is explicitly engineering bath atomic properties and compositions (e.g. masses, bond strengths), which works well for toy model studies<sup>43</sup> and is much more straightforward computationally. For the purpose of this study, we will choose the latter strategy as laid out specifically below.

Consider the case where the colored bath consists of  $N$  atoms arranged in a linear chain (See Fig. 2). We want the atom number 0 to represent a Debye bath effect. We start by regarding the system without the molecule. The potential for bilinear interactions can be written as (in 1-dimensional notations):

$$V(x_0, x_1, \dots, x_N) = \frac{1}{2} \sum_{j=1}^N \sum_{l=1}^N K_{jl} x_j x_l \quad (15)$$

$$\frac{d^2 x_n}{dt^2} = -\frac{1}{M_n} [K_{n,n+1} x_{n+1} + K_{n,n-1} x_{n-1} + K_{nn} x_n]; \quad (16)$$

$$n \neq 0, N$$

The last atom (N) is connected to white noise,

$$\begin{aligned} \frac{d^2x_N}{dt^2} &= \frac{1}{M_N} [K_{N,N-1}x_{N-1} + K_{NN}x_N] \\ &\quad - \gamma \frac{dx_N}{dt} + \frac{1}{M_N} R(t), \\ \langle R(t)R(0) \rangle &= 2M_N\gamma k_B T \delta(t). \end{aligned} \tag{17}$$

After mathematical transformations and derivations (see details in Appendix B), the spectrum density of the explicit bath,

$$g(\omega) = |[\mathbf{M}^{-1}]_{0N}|^2 \omega^2 \frac{3\gamma}{\pi^2}, \tag{18}$$

where  $\mathbf{M}$  is the dynamical force and frequency related matrix defined in Appendix B.

With parameters of force constants (i.e.  $k_{ij}$ ) and the coupling ( $\gamma$ ), we can fit the density of modes into Debye-shape (with a normalization factor C),

$$g(\omega) = C \frac{\omega^2}{1 + (\omega/\omega_D)^{2(N+1)}}, \tag{19}$$

which shows in the same form of the math filter method.<sup>42</sup>

As an example of the above formalism, we will use two layers (one atom for each layer) of representative bath atoms that give rise to the eighth power of  $\omega$  when fitted into Eq. 19 (with specific tunable parameters), which could be a good estimator for the purpose of simple model investigations. It can be shown the specific values for the tuning parameters can be calculated (details in Appendix B).

TABLE I. Molecular dynamics simulation parameters for various models studied in this work in the reduced units. Using the symbol  $\bar{\omega}$  for the diatomic molecule's internal vibrational frequency, the frequency mode associated with the reduced Debye frequency is set as  $\omega_D = 4\bar{\omega}$  (value calculated in Eq. B32). The force constants inside the Debye baths,  $k_1$  and  $k_2$  are the reduced spring constants associated with the bath atoms arranged in a linear chain, the last of which is connected to the white bath with a reduced friction coefficient of  $\gamma$ . See Appendix B for detailed derivations.

Quasiclassical Bath	$k_1$	$k_2$	$\gamma$	Random Noise
	$17.21\bar{\omega}^2$	$14.95\bar{\omega}^2$	$9.26\bar{\omega}$	Eq. 13
System: Diatomic Molecule	$k_0$			
	$\bar{\omega}^2$			
System: 1D-Polymer	$k_0$ (Eq. 20)			
	$11.37\bar{\omega}^2$			
System-Bath: Harmonic	$k_R$	$k_L$		
	$0.23\bar{\omega}^2$	$0.23\bar{\omega}^2$		
System-Bath: Morse	$\alpha$	$D$	$2\alpha^2 D$	
	$0.33\sqrt{\bar{\omega}/\hbar}$	$1.06\hbar\bar{\omega}$	$0.23\bar{\omega}^2$	

### III. SIMPLE APPLICATIONS: RELAXATION OF A SINGLE HARMONIC OSCILLATOR

We start by applying the QCET approach to the relaxation dynamics of a single oscillator, representing a diatomic molecule, coupled to a harmonic heat bath as shown in Fig. 3.

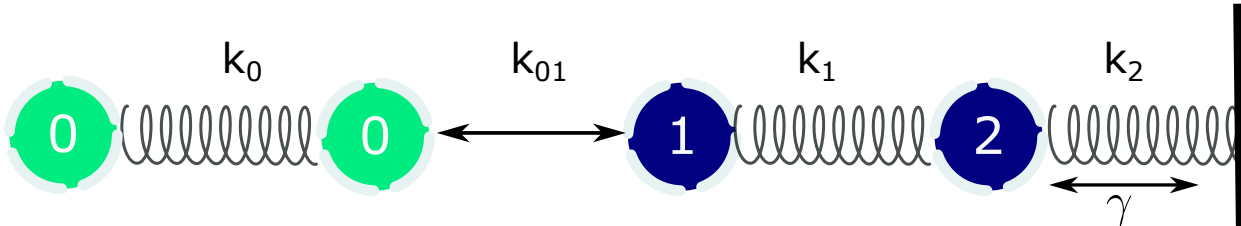


FIG. 3. Schematic drawing of the diatomic molecule attached to a colored bath represented by two harmonically bonded atoms and a thermal reservoir. The molecule is represented on the left by the number 0, connected to the bath atoms, which are parameterized according to Table I.

Making use of the analytical expressions for both classical and quantum equilibrium energies of harmonic and anharmonic (Morse) oscillators (see Fig. S2 and S3 in SI. Note that SI is separate from the appendices), we simulate the relaxation processes of both the classical MD approach and the QCET dynamics approach (Eq. 13) we have developed and compare them to the available analytical results.

The simulation of QCET, which considers quantum effect of the reservoirs, can account for both high and low temperature limits at equilibrium, by encoding an effective temperature that incorporates quantum boson distribution into the molecular dynamics (see Fig. S1 in SI). To show the effect of colored-Debye bath and anharmonicity within the capacity of the QCET method, we simulate the energy relaxation of a diatomic molecule coupled to the bath surface. Here, we use different interactions and parameters (see Table I and Fig. 3) to show the rates of energy relaxation for such a model with respect to bath temperature

changes.

Two types of interactions are taken between the molecule and the bath (i.e. between atom 0 and 1). a). Harmonic ( $k_{01} = 0.23\bar{\omega}$  as default); b). Anharmonic (Morse potential details in Section I and Section III in SI). Figure 4 shows energy relaxation for the harmonic oscillator within the range of Debye spectrum. Initial states of the oscillator are sampled from the same total energy with random displacements and velocities. The relaxation energy is calculated as the difference between the statistical ensemble averages of the time-dependent total energy changes and the energy when the system is equilibrated to the bath. While in the classical case the temperature is constant, the effective temperature for the QCET comes from the collective effect of phonons in the quantum bath that follows Bose-Einstein distribution. That is why the quasiclassical appears slightly higher than the classical line, because the equilibrium energy of the augmented quantum bath is smaller caused by overall lower effective temperature. As the energy decays exponentially, we can do logarithmic fits to get the relaxation rates from the slopes. It is shown that the classical and quantum cases align with each other well ( $\sim 0.0002$  in Fig. 4). However, it is not exactly the same for anharmonic interface potentials (see Section IV in SI for detailed results). At higher vibrational frequencies, the anharmonic (Morse) potential generates higher rates than the harmonic potential when connected to a Debye-colored bath, shown from the QCET simulations.

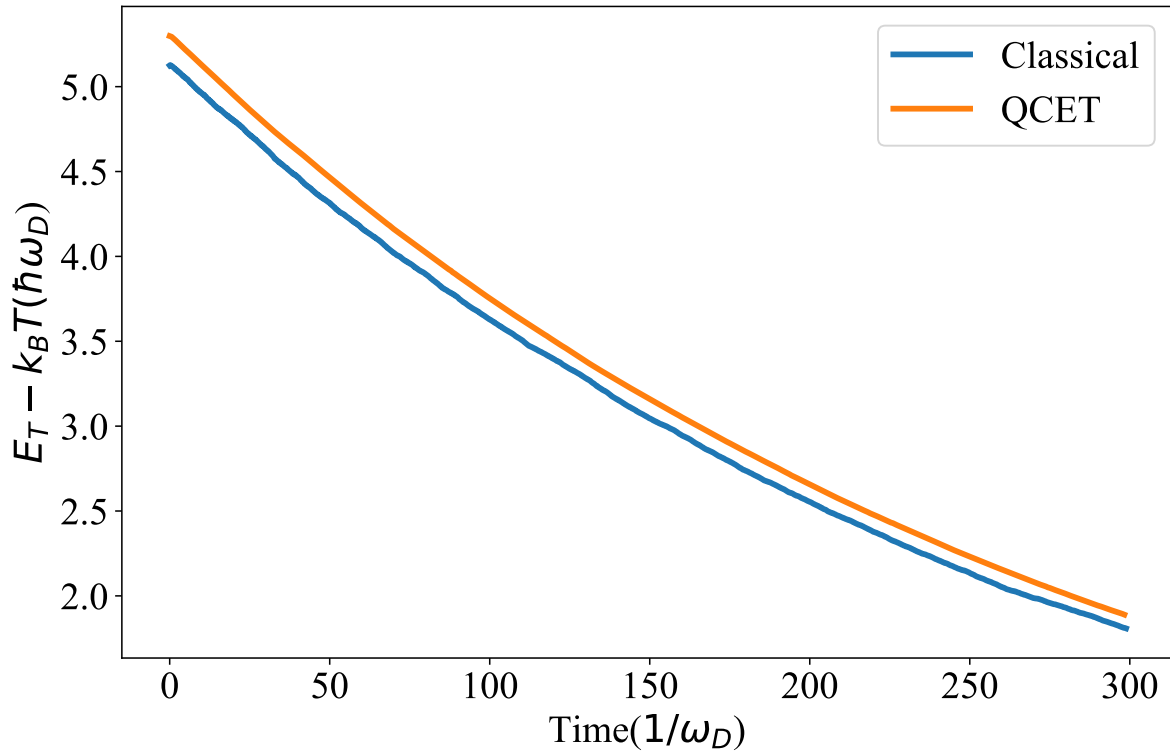


FIG. 4. Examples of energy relaxation rates of the diatomic molecule shown in Fig. 3, with classical and QCET method. The internal vibration frequency is 1/4 of Debye cutoff and temperature is 0.2 ( $\hbar\omega_D/k_B$ ). The horizontal axis is the evolution time. The slopes of the logarithmic fits of the energy changes (vertical axis values) are 0.000209 for the classical and 0.000207 for the quantum, which correspond to their relaxation rates respectively.

#### IV. HEAT CONDUCTION BETWEEN DEBYE THERMAL BATHS

In this Section, the heat conduction is investigated for a diatomic molecular system and a one-dimensional polymeric system all under engineered Debye-colored baths (see Section II B). Figure 5 shows the results from classical MD simulations and QCET simulations for a diatomic molecular system. All the parameters are set to be the same for Debye bath as described in Section II B, only now we have two baths with different temperatures.

A few observations can be made for the diatomic molecule heat conduction with harmonic couplings to the baths in Fig. 5 (lower three lines): (a) The heat current from the classical MD approach is almost T-independent across the low, middle to high bath temperatures, as long as the biases are kept the same. (b) The Landauer’s calculation reduces to about half of the value at lower temperature limit compared to the constant temperature case (the reason it does not go to zero is that thermal bias always provides transporting phonons in the right bath even when the left bath has close-to-zero temperature), and catches up gradually as temperature rises. The trend of the QCET aligns well with the Landauer’s results. (c) All three approaches converge to the same values, as temperature of the left bath becomes high, which is expected that quantum effect reduces to its minimum at the classical (high-T) limit.

The Landauer’s calculations depict accurate behaviors for pure harmonic systems for the full temperature range, while the classical MD results act as its approximation for high-T limit (similar behaviors can be shown with white baths as well for diatomic small molecules. See Fig. S4 in SI for details). By showing the agreement of the QCET method to the Landauer’s calculation, we confirm indeed that this method is capable of capturing full dynamics of the molecular heat conduction, through carefully engineering the bath



properties to introduce the Bose-Einstein distribution of quantum mechanical phonons.

Nonetheless, for heat conduction in anharmonic systems, one will need to rely solely on simulational approaches for accurate depictions of heat transport features. After replacing harmonic molecule-bath couplings with anharmonic (Morse) couplings (detailed Hamiltonians are shown in Section VI in SI), the currents (top two lines) increase from 30% to 60% for all bath temperatures, indicating the higher-order anharmonicities participate the thermal transport processes and enhance the overall conducting effects. More interestingly, comparing between the classical anharmonic and QCET anharmonic results, there is an increase for high temperature conduction for the quantum data, which could be a combined effects from quantum statistical distributions and anharmonic interactions from outside the Debye spectrum. Such an enhancement which is absent from the classical counterparts also agrees with the observations from the energy relaxation processes (see Fig. S2 and S3 in SI), which further infers under the QCET model, we are able to capture anharmonic system-bath coupling effects and quantum populations of molecular heat transport that are not available to either full quantum harmonic calculations (e.g. Landauer) or classical MD simulations. It is worth noting that Ref. 40 attributes the slight decrease of higher-temperature conduction for alkanes to anharmonicity in the molecules, while in fact for their junction systems, with multiple layers of substrates such deduction could also come from inelastic scattering events at the interface, which increase the resistance of the junctions to heat flow. In a relevant study, Xufei *et al.*<sup>45</sup> report the increase in the thermal conductance of monoatomic or diatomic lattices as the anharmonicity is increased. However, they report that tuning the anharmonicity right at the interface does not show obvious effects on the the thermal conductance. Therefore, there are too many contributing factors interweaving with each other that it is not possible to explain the outcome from a dominant factor. We show here through

our simple anharmonic model, anharmonicities do not necessarily contribute to the reduced thermal conduction at higher temperatures. On the contrary, Morse-type potentials result in enhancement of conduction, which could be illustrated by our newly developed QCET MD simulations.

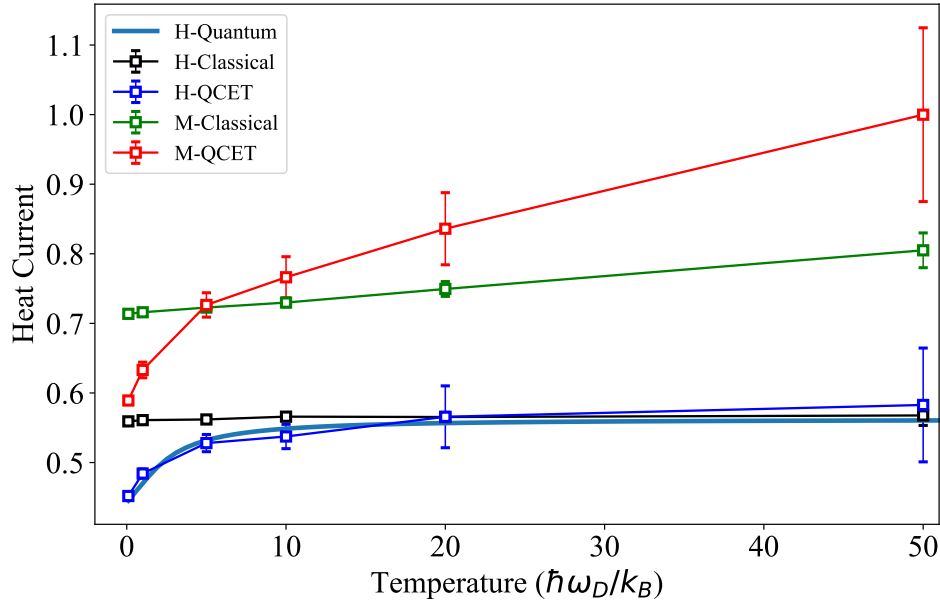


FIG. 5. Heat currents of the diatomic molecular system connected to engineered Debye baths (specified in Fig. 3) one on the left and one on the right, with two different interactions between the system and baths, namely, harmonic (represented as H in the legend) and Morse (one example of anharmonic system-bath interactions, represented as M in the legend, see Section III in SI for details). Quantum denotes Landauer-based quantum calculations. The parameters for left and right baths are the same (Table I), except the temperatures (the left bath temperatures are shown on the x-axis, and the right bath is always  $20 \hbar\omega/k_B$  higher than the left bath). The internal vibrational frequency for the diatomic molecule is  $1/4$  of the Debye cutoff (Eq. B32) of the baths, and the coupling between the bath and the molecule is  $k_{01} = 0.007\omega_D^2$ . For the Morse (anharmonic) interaction, the parameters are chosen such that  $k_{01} = 2\alpha^2 D$ . (see Section III in SI). The y-axis is normalized by the current of anharmonic quantum data at  $70 \hbar\omega/k_B$ . The error bars represent Standard Error.<sup>44</sup>

Finally, the heat conduction is investigated for one-dimensional polymer chains placed between two colored baths (See Section I of SI for the Hamiltonian of this type of junction). The one-dimensional polymer chains consists of  $N$  units with the same mass ( $m$ ) and spring constant ( $k_0$ ) leading to the following equations of motion for the  $n$ th unit in the polymer chain:

$$m\ddot{x}_n = \begin{cases} -2k_0x_1 + k_0x_2 + F_L, & n = 1 \\ k_0x_{n-1} - 2k_0x_n + k_0x_{n+1}, & 1 < n < N \\ -2k_0x_N + k_0x_{N-1} + F_R, & n = N \end{cases} \quad (20)$$

where  $F_L$  and  $F_R$  represent the left and right bath forces to the closest units/atoms in the one-dimensional polymer, respectively. The same equations of motion for the (quantum augmented) bath as presented in Section II A is used with two atoms to represent the bath (see Fig. 3) and the polymer-bath coupling parameter as well as the temperature difference between baths are the same as the ones used for the diatomic case above (see Table I). To address the significance of the quantum augmented colored bath, one may compare the heat currents to the ones obtained in a classical colored bath, which is implemented by reducing the effective temperature in Eq. 14 to the bath temperature.

The blue filled circles in Fig. 6 show the dependence of the heat current on chain length for one-dimensional polymer chains consisting of 1–20 units coupled to quantum augmented colored bath at a temperature of  $20 \hbar\omega/k_B$  for the lower bath (with bias being  $2 \hbar\omega/k_B$ ). As can be seen, the heat current has minimal length dependent for  $N > 10$ , while for short chains, a rise of the heat conductance with chain length is observed. The red filled squares in Fig. 6 show the chain length dependence for one-dimensional polymer chains coupled to classical colored baths. All the results are normalized with the heat current value for

the one-dimensional polymer chain with  $N = 1$  coupled with the classical colored bath. As can be seen, a similar trend is observed for the chain length dependence of polymer chains coupled to the classical bath noting that the heat currents from the classical baths are the upper heat current values when compared to the ones obtained from the quantum bath, which shows the intrinsic working of Bose-Einstein quantum populations in lowering the overall effective temperatures.

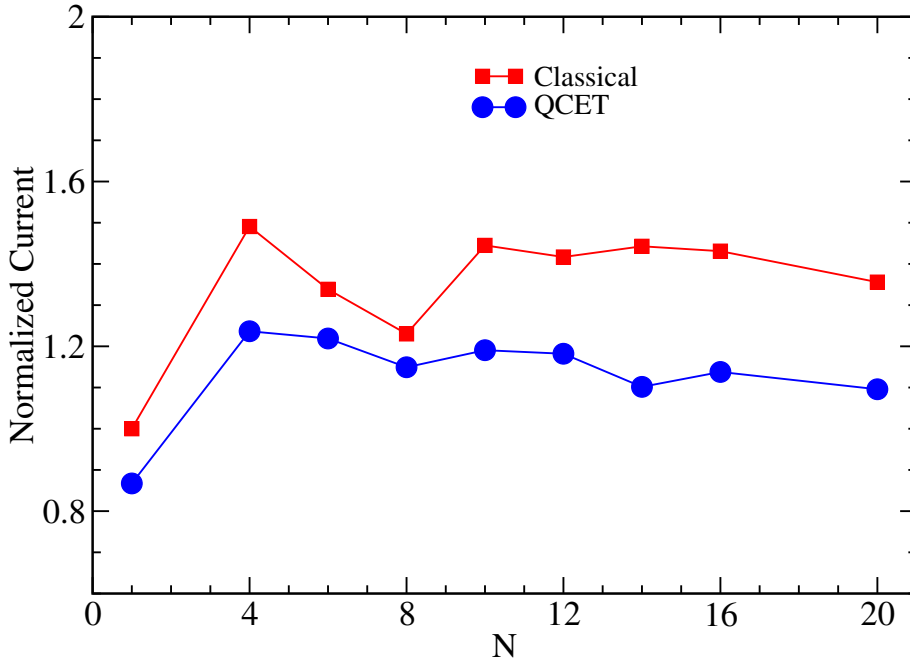


FIG. 6. Normalized heat current at a reduced temperature of  $20 \hbar\omega/k_B$  for the lower bath (with bias being  $2 \hbar\omega/k_B$ ) for a one-dimensional polymer chain with various chain lengths coupled to classical or quasiclassical baths (see Fig. 3). All the currents are normalized with respect to the heat current value of a molecule with  $N = 1$  coupled to the classical bath.

## V. CONCLUSION

As we have pointed out in the development of stochastic nonequilibrium simulation of molecular heat conduction<sup>37</sup>, the inadequacy of describing thermal population of phononic modes may have been the main reason leading to the failure of accurate depiction of low-temperature thermal conductance of single-molecule junctions under classical MD. Indeed, in this article we have augmented the conventional atomistic simulation for molecular heat conduction with quantum phononic baths, in which the quantum thermal transport features are effectively incorporated into the dynamics while at the same time the advantages of classical MD (e.g. full force-field interactions) is retained. Such a successful augmentation has been first demonstrated through monatomic equilibration and diatomic molecular junction heat conduction. In both scenarios we have seen the asymptotic behaviors of the quantum bath method at the high-temperature limit always converge to the classical approaches, while at the low-temperature end they align with quantum analytical expressions and Landauer's transport calculations. We have thus overcome the shortcomings of classical MD in simulating the molecular heat conduction when quantum effects may be significant, with relatively small added computational complexity. We have also introduced colored bath into the quantum bath method to account for spectral features of contacting substrates (e.g. gold) in the junctions and full-range of vibrational modes in the molecular bridges. Our results in Fig. 5 indicate the anharmonicity in the systems (modeled by Morse potential) might increase or decrease the heat conductance because of the interactions and scatterings of all the normal modes in the systems, which could be utilized to modulate heat conduction by introducing or hybridizing different molecular structures. The chain length dependence of heat current is also investigated for one-dimensional polymer chains coupled to quantum

and classical colored baths. It is found that the heat currents for the colored classical baths are the upper values for the quantum augmented baths and both show minimal chain length dependence for polymer chains with more than 10 units while the chain length dependence for polymer chains with less than 10 units is significant. For the future work direction, the implementation of this method to the existing MD simulation package will be done for the full exploration of molecular thermal transport covering all extreme conditions (e.g. heat conduction of large systems like polymer chains<sup>46</sup> at low and high ambient temperatures). Such efforts may verify and guide experimental studies in these directions and prepare for the future applications in molecular phononics.

## **VI. SUPPLEMENTARY INFORMATION**

The the Hamiltonian of the junctions as well as the complementary analytical expressions for one-dimensional oscillators, anharmonic effects on the relaxation of Morse oscillators, diatomic molecule white-noise heat conduction, and Debye bath features are presented in the supplementary information.

## **VII. ACKNOWLEDGMENTS**

This work was supported by the U.S. National Science Foundation under Grant No. CHE1953701 and by the University of Pennsylvania. R.C. acknowledges the support from the Center for Nonlinear Studies (CNLS) as a postdoctoral fellow at the Los Alamos National Laboratory (LANL). M. D. acknowledges the support from the U.S. Department of Energy, Office of Basic Energy Sciences, Division of Chemical Science, Geosciences, and Biosciences at Pacific Northwest National Laboratory (PNNL).

## **VIII. DATA AVAILABILITY**

The data that supports the findings of this study are available within the article and its supplementary material. Source code implementations are also available from the corresponding author upon reasonable request.



## Appendix A: Dimensionless units

All the dimensionless variables are defined as follows in terms of harmonic oscillator frequency (included Morse potential parameters):

$$\begin{aligned}
 \bar{x} &= \frac{x}{\sqrt{\frac{\hbar}{m\omega}}} \\
 \bar{v} &= \frac{v}{\sqrt{\frac{\hbar\omega}{m}}} \\
 \bar{\omega}_n &= \frac{\omega_n}{\omega} \\
 \bar{t} &= \omega t \\
 \bar{\gamma} &= \frac{\gamma}{\omega} \\
 \bar{T} &= \frac{\hbar\omega}{k_B T} \\
 \bar{T}_{eff}^{(n)} &= \frac{\bar{\omega}_n}{e^{\bar{\omega}_n/\bar{T}-1}} \\
 \bar{D} &= \frac{D}{\hbar\omega} \\
 \bar{\alpha} &= \alpha \sqrt{\frac{\hbar}{m\omega}}
 \end{aligned} \tag{A1}$$

## Appendix B: Derivations of parameters for explicit layers Debye bath model

In mass-weighted coordinates, one gets

$$\frac{d^2 y_n}{dt^2} = -(k_{n,n+1} y_{n+1} + k_{n,n-1} y_{n-1} + k_{nn} y_n); \tag{B1}$$

$$n \neq 0, N$$

$$\frac{d^2 y_0}{dt^2} = -(k_{0,1} y_1 + k_{00} y_0) \tag{B2}$$

$$\frac{d^2 y_N}{dt^2} = -(k_{N,N-1} y_{N-1} + k_{NN} y_N) - \gamma \frac{dy_N}{dt} + \rho(t), \tag{B3}$$

where we have defined,

$$y_n = \sqrt{M_n}x_n, \quad k_{ij} = \frac{K_{ij}}{\sqrt{M_i M_j}}, \quad (\text{B4})$$

$$k_{nn} = \frac{K_{nn}}{M_n}, \quad \rho(t) = \frac{R(t)}{\sqrt{M_N}},$$

$$\langle \rho(t)\rho(0) \rangle = 2\gamma k_B T \delta(t). \quad (\text{B5})$$

Now as we transform to Fourier space,

$$f(t) = \tilde{f}(\omega)e^{-i\omega t} + \tilde{f}(-\omega)e^{i\omega t} \quad (\text{B6})$$

We have,

$$\omega^2 \tilde{y}_0 = k_{01} \tilde{y}_1 + k_{00} \tilde{y}_0 \quad (\text{B7})$$

$$\omega^2 \tilde{y}_n = k_{n,n+1} \tilde{y}_{n+1} + k_{n,n-1} \tilde{y}_{n-1} + k_{nn} \tilde{y}_n \quad (\text{B8})$$

$$\omega^2 \tilde{y}_N = k_{N,N-1} \tilde{y}_{N-1} + k_{NN} \tilde{y}_N - i\omega\gamma \tilde{y}_N - \tilde{\rho}(\omega). \quad (\text{B9})$$

We may further put them into matrix form.

$$\mathbf{M}\mathbf{y} = \mathbf{r}, \quad (\text{B10})$$

where

$$\mathbf{r} = \begin{bmatrix} 0 \\ 0 \\ \vdots \\ \tilde{\rho} \end{bmatrix} \quad (\text{B11})$$

$$\mathbf{M} = \begin{bmatrix} k_{00} - \omega^2 & k_{01} & \dots & 0 \\ k_{10} & k_{11} - \omega^2 & k_{12} & 0 \\ \vdots & \vdots & \ddots & \vdots \\ 0 & \dots & k_{N,N-1} & k_{NN} - \omega^2 - i\omega\gamma \end{bmatrix} \quad (\text{B12})$$

The matrix can be inverted analytically,

$$\tilde{y}_0(\omega) = [\mathbf{M}^{-1}]_{0N} \tilde{\rho}(\omega) \quad (\text{B13})$$

whence we have

$$\langle |\tilde{y}_0(\omega)|^2 \rangle = |[\mathbf{M}^{-1}]_{0N}|^2 \omega^2 \langle |\tilde{\rho}(\omega)|^2 \rangle \quad (\text{B14})$$

$\tilde{\rho}(\omega)$  is the Fourier transform of the random noise  $\rho$  and its squared averaging equal to<sup>41</sup>

$$\langle |\tilde{\rho}(\omega)|^2 \rangle = \frac{\gamma k_B T}{\pi}, \quad (\text{B15})$$

note the mass is unity in the mass-weighted representation. We then have

$$\langle |\tilde{y}_0(\omega)|^2 \rangle = |[\mathbf{M}^{-1}]_{0N}|^2 \omega^2 \frac{\gamma k_B T}{\pi} \quad (\text{B16})$$

The LHS is the Fourier transform<sup>41</sup> of the velocity correlation function of the atom in the bath seen by the molecule.

When we connect the bath spectrum density to the v-v correlation<sup>41</sup>

$$g(\omega) = \frac{3mN}{\pi k_B T} \int_{-\infty}^{\infty} dt \langle \dot{x}(0) \dot{x}(t) \rangle e^{-i\omega t}. \quad (\text{B17})$$

We have the expression that takes into account the force constants matrix.

$$g(\omega) = |[\mathbf{M}^{-1}]_{0N}|^2 \omega^2 \frac{3\gamma}{\pi^2} \quad (\text{B18})$$

For two-atoms bath (see Fig. 3) the left atom of the bath was taken to couple to the molecule:

$$\mathbf{M} = \begin{bmatrix} k_{00} - \omega^2 & -k_1 \\ -k_1 & k_{11} - i\gamma\omega - \omega^2 \end{bmatrix} \quad (\text{B19})$$

$$k_{00} = k_1, \quad k_{11} = k_1 + k_2 \quad (\text{B20})$$

$$\det(\mathbf{M}) = \omega^4 + i\gamma\omega^3 - (2k_1 + k_2)\omega^2 - i\gamma k_1\omega + k_1k_2 \quad (\text{B21})$$

$$\mathbf{M}^{-1} = \frac{1}{\det(\mathbf{M})} \begin{bmatrix} k_1 + k_2 - i\gamma\omega - \omega^2 & k_1 \\ k_1 & k_1 - \omega^2 \end{bmatrix} \quad (\text{B22})$$

$$|\mathbf{M}^{-1}|_{12} = \frac{k_1}{\det(\mathbf{M})} \quad (\text{B23})$$

The denominator of  $(|\mathbf{M}^{-1}|_{12})^2$  is

$$\omega^8 + c_6\omega^6 + c_4\omega^4 + c_2\omega^2 + c_0 \quad (\text{B24})$$

where

$$c_6 = \gamma^2 - 2(2k_1 + k_2) \quad (\text{B25})$$

$$c_4 = (2k_1 + k_2)^2 + 2k_1k_2 - 2\gamma^2k_1 \quad (\text{B26})$$

$$c_2 = \gamma^2k_1^2 - 2k_1k_2(2k_1 + k_2) \quad (\text{B27})$$

$$c_0 = k_1^2k_2^2 \quad (\text{B28})$$

Under the condition,  $c_6 = c_4 = c_2 = 0$  and  $k_1 \neq 0$  and  $k_2 \neq 0$ , we fit the parameters

$$k_1 = 0.151388, \quad k_2 = 0.131483, \quad \gamma = 0.868517 \quad (\text{B29})$$

We can then go back to the expression of the density of modes,

$$g(\omega) = (|\mathbf{M}^{-1}|_{12})^2 \omega^2 \frac{3\gamma}{\pi^2} \quad (\text{B30})$$

and plot  $g(\omega)$ . If we assume

$$g(\omega) = C \frac{\omega^2}{1 + (\frac{\omega}{\omega_D})^8}, \quad (\text{B31})$$

then we have

$$\omega_D = (c_0)^{1/8} \approx 0.375126 \quad (\text{B32})$$

The spectrum is tested and confirmed with its Fourier transform of the auto-correlation functions to reflect the Debye cut-off characteristics.

## REFERENCES

- <sup>1</sup>D. G. Cahill, W. K. Ford, K. E. Goodson, G. D. Mahan, A. Majumdar, H. J. Maris, R. Merlin, and S. R. Phillpot, “Nanoscale thermal transport,” *J. Appl. Phys.* **93**, 793–818 (2003), doi:10.1063/1.1524305.
- <sup>2</sup>D. G. Cahill, P. V. Braun, G. Chen, D. R. Clarke, S. Fan, K. E. Goodson, P. Keblinski, W. P. King, G. D. Mahan, A. Majumdar, H. J. Maris, S. R. Phillpot, E. Pop, and L. Shi, “Nanoscale thermal transport. ii. 2003–2012,” *Appl. Phys. Rev.* **1**, 011305 (2014).
- <sup>3</sup>G. Benenti, G. Casati, K. Saito, and R. S. Whitney, “Fundamental aspects of steady-state conversion of heat to work at the nanoscale,” *Phys. Rep.* **694**, 1 – 124 (2017).
- <sup>4</sup>J. C. Cuevas and E. Scheer, *Molecular electronics: an introduction to theory and experiment* (World Scientific Series in Nanotechnology and Nanoscience, Singapore, 2010).
- <sup>5</sup>Y. Dubi and M. Di Ventra, “*Colloquium* : Heat flow and thermoelectricity in atomic and molecular junctions,” *Rev. Mod. Phys.* **83**, 131–155 (2011), doi:10.1103/RevModPhys.83.131.
- <sup>6</sup>D. Segal and B. K. Agarwalla, “Vibrational heat transport in molecular junctions,” *Annu. Rev. Phys. Chem.* **67**, 185–209 (2016).
- <sup>7</sup>L. Cui, R. Miao, C. Jiang, E. Meyhofer, and P. Reddy, “Perspective: Thermal and thermoelectric transport in molecular junctions,” *J. Chem. Phys.* **146**, 092201 (2017).
- <sup>8</sup>R. Chen, G. T. Craven, and A. Nitzan, “Electron-transfer-induced and phononic heat transport in molecular environments,” *The Journal of Chemical Physics* **147**, 124101 (2017).
- <sup>9</sup>G. T. Craven, D. He, and A. Nitzan, “Electron-transfer-induced thermal and thermoelectric rectification,” *Phys. Rev. Lett.* **121**, 247704 (2018).

- <sup>10</sup>Z. Wang, J. A. Carter, A. Lagutchev, Y. K. Koh, N.-H. Seong, D. G. Cahill, and D. D. Dlott, “Ultrafast flash thermal conductance of molecular chains,” *Science* **317**, 787–790 (2007), doi:10.1126/science.1145220.
- <sup>11</sup>N. I. Rubtsova, L. N. Qasim, A. A. Kurnosov, A. L. Burin, and I. V. Rubtsov, “Ballistic energy transport in oligomers,” *Acc. Chem. Res.* **48**, 2547–2555 (2015).
- <sup>12</sup>B. C. Pein, Y. Sun, and D. D. Dlott, “Unidirectional vibrational energy flow in nitrobenzene,” *J. Phys. Chem. A* **117**, 6066–6072 (2013).
- <sup>13</sup>H. Sadeghi, S. Sangtarash, and C. J. Lambert, “Oligoyne molecular junctions for efficient room temperature thermoelectric power generation,” *Nano Lett.* **15**, 7467–7472 (2015).
- <sup>14</sup>N. Li, J. Ren, L. Wang, G. Zhang, P. Hänggi, and B. Li, “*Colloquium* : Phononics: Manipulating heat flow with electronic analogs and beyond,” *Rev. Mod. Phys.* **84**, 1045–1066 (2012), doi:10.1103/RevModPhys.84.1045.
- <sup>15</sup>D. Segal, A. Nitzan, and P. Hänggi, “Thermal conductance through molecular wires,” *J. Chem. Phys.* **119**, 6840–6855 (2003).
- <sup>16</sup>R. Chen, I. Sharony, and A. Nitzan, “Local atomic heat currents and classical interference in single-molecule heat conduction,” *J. Phys. Chem. Lett.* **11**, 4261–4268 (2020).
- <sup>17</sup>T. Meier, F. Menges, P. Nirmalraj, H. Hölscher, H. Riel, and B. Gotsmann, “Length-dependent thermal transport along molecular chains,” *Phys. Rev. Lett.* **113**, 060801 (2014), doi:10.1103/PhysRevLett.113.060801.
- <sup>18</sup>S. Majumdar, J. A. Malen, and A. J. H. McGaughey, “Cooperative molecular behavior enhances the thermal conductance of binary self-assembled monolayer junctions,” *Nano Lett.* **17**, 220–227 (2017).
- <sup>19</sup>J. T. Gaskins, A. Bulusu, A. J. Giordano, J. C. Duda, S. Graham, and P. E. Hopkins, “Thermal conductance across phosphonic acid molecules and interfaces: Ballistic versus

- diffusive vibrational transport in molecular monolayers,” *J. Phys. Chem. C* **119**, 20931–20939 (2015).
- <sup>20</sup>S. Majumdar, J. A. Sierra-Suarez, S. N. Schiffrés, W.-L. Ong, C. F. Higgs, A. J. H. McGaughey, and J. A. Malen, “Vibrational mismatch of metal leads controls thermal conductance of self-assembled monolayer junctions,” *Nano Letters* **15**, 2985–2991 (2015), <https://doi.org/10.1021/nl504844d>.
- <sup>21</sup>L. Cui, S. Hur, Z. A. Akbar, J. C. Klöckner, W. Jeong, F. Pauly, S.-Y. Jang, P. Reddy, and E. Meyhofer, “Thermal conductance of single-molecule junctions,” *Nature* **572**, 628–633 (2019).
- <sup>22</sup>N. Mosso, H. Sadeghi, A. Gemma, S. Sangtarash, U. Drechsler, C. Lambert, and B. Gotsmann, “Thermal transport through single-molecule junctions,” *Nano Lett.* **19**, 7614–7622 (2019).
- <sup>23</sup>J. C. Klöckner, M. Bürkle, J. C. Cuevas, and F. Pauly, “Length dependence of the thermal conductance of alkane-based single-molecule junctions: An *ab initio* study,” *Phys. Rev. B* **94**, 205425–1–8 (2016).
- <sup>24</sup>L. Cui, W. Jeong, S. Hur, M. Matt, J. C. Klöckner, F. Pauly, P. Nielaba, J. C. Cuevas, E. Meyhofer, and P. Reddy, “Quantized thermal transport in single-atom junctions,” *Science* (2017), 10.1126/science.aam6622.
- <sup>25</sup>J. C. Klöckner, J. C. Cuevas, and F. Pauly, “Tuning the thermal conductance of molecular junctions with interference effects,” *Phys. Rev. B* **96**, 205425–1–10 (2017).
- <sup>26</sup>J. C. Klöckner, J. C. Cuevas, and F. Pauly, “Transmission eigenchannels for coherent phonon transport,” *Phys. Rev. B* **97**, 155432 (2018).
- <sup>27</sup>P. K. Schelling, S. R. Phillpot, and P. Keblinski, “Comparison of atomic-level simulation methods for computing thermal conductivity,” *Physical Review B - Condensed Matter*



- and Materials Physics **65**, 1–12 (2002).
- <sup>28</sup>D. P. Sellan, E. S. Landry, J. E. Turney, A. J. H. McGaughey, and C. H. Amon, “Size effects in molecular dynamics thermal conductivity predictions,” *Phys. Rev. B* **81**, 1–10 (2010).
- <sup>29</sup>A. McGaughey and M. Kaviani, “Thermal conductivity decomposition and analysis using molecular dynamics simulations. part i. lennard-jones argon,” *Int. J. Heat Mass Transf.* **47**, 1783 – 1798 (2004).
- <sup>30</sup>A. McGaughey and M. Kaviani, “Thermal conductivity decomposition and analysis using molecular dynamics simulations: Part ii. complex silica structures,” *Int. J. Heat Mass Transf.* **47**, 1799 – 1816 (2004).
- <sup>31</sup>L. Chen and S. Kumar, “Thermal transport in graphene supported on copper,” *J. Appl. Phys.* **112**, 043502 (2012).
- <sup>32</sup>M. Zhang, E. Lussetti, L. E. S. de Souza, and F. Müller-Plathe, “Thermal conductivities of molecular liquids by reverse nonequilibrium molecular dynamics,” *J. Phys. Chem. B* **109**, 15060–15067 (2005), <https://doi.org/10.1021/jp0512255>.
- <sup>33</sup>S. Tang and Y. Kulkarni, “The interplay between strain and size effects on the thermal conductance of grain boundaries in graphene,” *Appl. Phys. Lett.* **103**, 213113 (2013).
- <sup>34</sup>H. Dong, B. Wen, and R. Melnik, “Relative importance of grain boundaries and size effects in thermal conductivity of nanocrystalline materials,” *Sci. Rep.* **4**, 7037 (2014).
- <sup>35</sup>P. H. Nguyen, S.-M. Park, and G. Stock, “Nonequilibrium molecular dynamics simulation of the energy transport through a peptide helix,” *J. Chem. Phys.* **132**, 025102 (2010).
- <sup>36</sup>S.-W. Hung, G. Kikugawa, and J. Shiomi, “Mechanism of temperature dependent thermal transport across the interface between self-assembled monolayer and water,” *J. Phys. Chem. C* **120**, 26678–26685 (2016).

- <sup>37</sup>I. Sharony, R. Chen, and A. Nitzan, “Stochastic simulation of nonequilibrium heat conduction in extended molecular junctions,” *J. Chem. Phys.* **153**, 144113 (2020).
- <sup>38</sup>P. Carpio-Martínez and G. Hanna, “Quantum bath effects on nonequilibrium heat transport in model molecular junctions,” *J. Chem. Phys.* **154**, 094108 (2021).
- <sup>39</sup>J.-S. Wang, “Quantum thermal transport from classical molecular dynamics,” *Phys. Rev. Lett.* **99**, 160601 (2007).
- <sup>40</sup>G. Li, B.-Z. Hu, N. Yang, and J.-T. Lü, “Temperature-dependent thermal transport of single molecular junctions from semiclassical langevin molecular dynamics,” *Phys. Rev. B* **104**, 245413 (2021).
- <sup>41</sup>A. Nitzan, *Chemical Dynamics in Condensed Phases: Relaxation, Transfer and Reactions in Condensed Molecular Systems* (Oxford University Press, 2006).
- <sup>42</sup>A. Nitzan, M. Shugard, and J. C. Tully, “Stochastic classical trajectory approach to relaxation phenomena. ii. vibrational relaxation of impurity molecules in debye solids,” *J. Chem. Phys.* **69**, 2525–2535 (1978).
- <sup>43</sup>N. Kalantar, B. K. Agarwalla, and D. Segal, “Harmonic chains and the thermal diode effect,” *Phys. Rev. E* **103**, 052130 (2021).
- <sup>44</sup>D. G. Altman and J. M. Bland, “Standard deviations and standard errors,” *BMJ (Clinical research ed.)* **331**, 903 (2005).
- <sup>45</sup>X. Wu and T. Luo, “The importance of anharmonicity in thermal transport across solid-solid interfaces,” *Journal of Applied Physics* **115**, 014901 (2014).
- <sup>46</sup>M. Dinpajoo and A. Nitzan, “Heat conduction in polymer chains: Effect of substrate on the thermal conductance,” *J. Chem. Phys.* **156**, 144901 (2022).